Journal of Materials Chemistry A

Accepted Manuscript

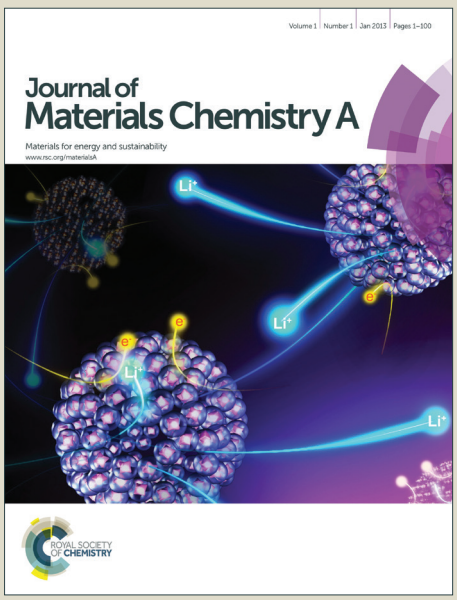

ROYAL SOCIETY OF CHEMISTRY

www.rsc.org/materialsA

Thermoelectric properties of Cu_3SbSe_3 with intrinsically ultralow lattice thermal conductivity

Kriti Tyagi[a], Bhasker Gahtori[a], Sivaiah Bathula[a], A. K. Srivastava[a], A. K. Shukla[a], Sushil Auluck[a] and Ajay Dhar[a,*]

[a]CSIR-Network of Institutes for Solar Energy, CSIR-National Physical Laboratory, Dr. K. S. Krishnan Marg, New Delhi -110012, India

Abstract

We report the synthesis, characterization and thermoelectric property evaluation of Cu_3SbSe_3 with a view to explore its utility as an useful thermoelectric material, owing to its intrinsically low thermal conductivity. Cu_3SbSe_3 was synthesized employing solid state reaction process followed by spark plasma sintering and the synthesized material was extensively characterized for its phase, composition and structure, which suggested formation of a single-phase. The measured electrical transport properties of Cu_3SbSe_3 indicated a p-type conduction in this material. The electrical transport behavior augurs well with that predicted theoretically using first-principle density-functional theory calculations, employing generalized gradient approximation. The measured thermal conductivity was found to be 0.26 $Wm^{-1}K^{-1}$ at 550 K, which is the lowest, reported thus far for Cu_3SbSe_3 and is among the lowest for state-of-the-art thermoelectric materials. Despite its ultralow thermal conductivity, coupled with a moderate Seebeck coefficient, the calculated value of its thermoelectric figure-of-merit was found to be exceptionally low (< 0.1), which was primarily attributed to its low electrical conductivity. Nevertheless, it is argued that Cu_3SbSe_3, due its environmentally-friendly constituent elements, its ultralow thermal conductivity and moderate

* Corresponding author. Tel.: +91-11-45609456, Fax: +91-11-45609310
E-mail address: adhar@nplindia.org (Dr. Ajay Dhar)

thermopower, could be a potentially useful thermoelectric material as the power factor can be favorably tailored employing carrier concentration tuning using suitable metallic dopants.

1. Introduction

Thermoelectric devices can play an important role in generation of green energy and hence this technology is fast emerging as an alternative to other existing renewable sources of energy.[1-3] The efficiency of a thermoelectric device is mainly determined by the material's dimensionless figure-of-merit, $ZT=(\alpha^2\sigma/\kappa)T$, where α, σ, T are the Seebeck coefficient, electrical conductivity, absolute temperature and κ *is* the total thermal conductivity respectively. Further κ consists of contributions both from electronic (κ_e) and lattice (κ_L) part ($\kappa=\kappa_L+\kappa_e$). Clearly ZT can be enhanced either by increasing the power factor ($\alpha^2\sigma$) or decreasing κ, although concurrently altering both these parameters favorably would be the ideal situation. It has been experimentally established that in order to enhance ZT, reducing κ has been found to be a more experimentally plausible strategy, which has been successfully demonstrated for several thermoelectric materials. Different reported proof-of-principle studies in this direction include, synthesizing parent nano-crystalline materials[4]; *in situ* forming nanoscale dots[5]; precipitating nano-phases[6]; and artificially introducing nano-particles[7]. As is clearly evident, most of these techniques involve some kind of nanostructuring-based approach which, broadly speaking, can induce reduction in κ_L by enhanced scattering of heat-carrying phonons[8-11] by high density of nano-scale features of nearly comparable dimensions, apart from introducing some other favorable effects. However, if the resulting size of the nano-features, which generally arise as a result of nanostructuring, including, grain boundaries, defects, residual porosity is very low (~ 10 nm) then these can also scatter electrons, thus decreasing the electrical conductivity and nullifying the favorable effect of nanostructuring in enhancing ZT. In view of this, an alternative strategy is to develop thermoelectric materials with intrinsically low thermal conductivity, such as,

$AgSbTe_2$ (κ~0.39 $Wm^{-1}K^{-1}$, ZT~1.6 at 673 K)[12], Ag_9TlTe_5 (κ~0.22 W m^{-1} K^{-1}, ZT~1.2 at 700 K),[13] $AgCrSe_2$ (κ~0.20 W m^{-1} K^{-1}, ZT~1.0 at 800 K)[14] and $Ag_{0.95}GaTe_2$ (κ~0.20 W m^{-1} K^{-1}, ZT~0.7 at 850 K).[15] The low thermal conductivity in these materials is primarily due to strong lattice anharmonicity caused by the presence of non-bonded valence electrons in the sp-hybridized bonding orbitals.[16, 17] Recently, the ultralow thermal conductivity reported in thermoelectric SnSe (κ~0.23 W m^{-1} K^{-1}, ZT~2.6 at 973 K) has also been attributed to the anharmonic and anisotropic bonding.[18] However, similar behavior is also observed in Cu-Sb-Se based ternary compounds, particularly Cu_3SbSe_3, which exhibits a very low thermal conductivity, which is less than most of other chalcogenide-based thermoelectric compounds.[19] In Cu_3SbSe_3 compound, Sb is in +3 valence state, leaving two un-bonded 5s valence shell electrons (lone pairs). These electrons, due to their large polarizability, can give rise to strong anharmonicity (leading to strong phonon-phonon scattering) in Cu_3SbSe_3 resulting in their intrinsically low thermal conductivity.[20] Thus, the intrinsically low thermal conductivity in Cu_3SbSe_3, consisting of cost-effective elements, could be exploited for designing Cu_3SbSe_3 based efficient thermoelectric devices.

Surprisingly, despite its intrinsically low reported[17] κ and theoretically predicted ZT ~ 0.7,[21] there are no reports in the literature on its electrical transport and thermoelectric properties, although its electronic structure[22, 23] and κ[17, 24] have been investigated by several research groups. This seems to stem from the fact that it is difficult to synthesize single-phase Cu_3SbSe_3 and has only been attempted by a few researchers,[17, 25, 26] although several reports exist on the successful synthesis of its counterpart thermoelectric Cu_3SbSe_4.[27, 28]

Dat Do et. al.,[22] have been studied the underlying principles of band gap formation in both Cu_3SbSe_4 and Cu_3SbSe_3 and theoretically predicted the latter to be a better n-type thermoelectric material. Sevik and Cagin[21] have calculated the thermoelectric properties of Cu_3SbSe_3 using density-functional theory (DFT) and Boltzmann transport theories and predicted a ZT ~ 0.7 at 600 K for a p-

type material. Similar theoretical calculations performed by Zhang et al.,[23] suggest a positive value of Grüneisen parameter indicating a strong anharmonicity and these authors found a good agreement between their theoretically calculated κ and experimentally measured values reported earlier.

Skoug et al.,[17] reported the synthesis of Cu_3SbSe_3 employing directional fusion technique but its single-phase formation was not substantiated by the authors, neither by X-ray diffraction (XRD) nor any other characterization data. However, these authors observed a low thermal conductivity due to strong anharmonic phonon interactions and complex crystal structure, based on which it was thought to be a good thermoelectric material. Later, Kirkham et al.,[25] also reported the synthesis of Cu_3SbSe_3 employing vacuum melting technique but observed the presence of $CuSbSe_2$ and Cu_2Se phases in addition to the desired phase,[25] although they could finally obtain a single-phase material after subsequent heat-treatment for more than 72 hours. Recently, Liu et al.,[26] have also reported the colloidal synthesis of Cu_3SbSe_3 nano-crystals using hot injection method, which is a multi-step chemical process, however, these authors have not reported their thermoelectric transport properties. Thus, it is apparent that although some efforts have been made towards synthesizing Cu_3SbSe_3, but there are no reported experimental studies on their electrical transport or thermoelectric properties, in absence of which it is difficult to ascertain its earlier reported utility as a good thermoelectric material.[17]

In this paper we present a comprehensive study on the synthesis, characterization and thermoelectric property evaluation of Cu_3SbSe_3, synthesized using solid-state reaction in vacuum followed by spark plasma sintering (SPS). The synthesized material was characterized for its phase, structure and composition employing XRD, field emission scanning electron microscopy (FESEM), high resolution transmission electron microscopy (HRTEM), energy dispersive X-ray spectroscopy (EDXS) X-ray photoelectron spectroscopy (XPS) and differential scanning calorimeter (DSC). These detailed characterization results clearly confirmed the formation of Cu_3SbSe_3 in a single-phase

and the structure was in agreement with the earlier reported results.[29] The electrical transport measurement results indicate that the as-synthesized Cu_3SbSe_3 shows a p-type behavior in the measured temperature range of 300-550 K. Electronic band structure of Cu_3SbSe_3 has been evaluated using first-principle DFT calculations and the electrical transport properties were theoretically calculated using Boltzmann transport theory. These theoretical predicted values of α and σ were found to be in reasonable agreement with the experimental results. The measured κ was found to be 0.26 $Wm^{-1}K^{-1}$ (550 K), which is the lowest value reported for this material. However, despite an ultralow κ and moderate value of α, the calculated ZT was abysmally low (< 0.1) even at the highest temperature of measurement, which is contrary to the previously reported proposition.[21] Nevertheless, it is suggested that this material could possibly be a good potential thermoelectric material owing to its ultralow κ coupled with a reasonable value of α, as the power factor can be tailored favorably by employing carrier concentration tuning using suitable metallic doping.[30, 31]

2. Experimental Details

High-purity Cu, Sb and Se powders were weighed in proper stoichiometric ratio and ground thoroughly in a glove-box under a high-purity argon atmosphere. The powders were subsequently pelletized and vacuum-sealed (10^{-4} Torr) in a quartz tube. The sealed quartz ampoule was placed in a box furnace, heat-treated at 320°C for 96 hrs, and then furnace cooled to room temperature. This ingot was pulverized and the resulting powder was consolidated and sintered under vacuum (~4 Pa) using SPS (SPS Syntex, 725) at a pressure of 60 MPa at 300°C for 5 minutes (soaking time) at a heating rate of 300°C/minute using cylindrical graphite die with a 12.7 mm central opening diameter to obtain cylindrical disks. Phase purity and its identification were carried out using XRD (Rigaku, Miniflex-II) with a CuK_α source with Ni filter. The XRD patterns were collected with a step size of 0.02^o and scan rate of 2° per minute. HRTEM experiments were performed employing using a Tecnai G2 F30 STWIN operated at the electron accelerating voltage of 300 kV using electron source

as field emission electron gun. Specimens for electron microscopy were prepared by employing mechanical polishing followed by subsequent ion milling. Mechanical polishing was finally carried out by thinning of a 3 mm diameter disc of specimen of about 50 to 100 μm down to a thickness of about 20 to 30 μm by utilizing a dimple grinder (model: 515 CE, South Bay Technology). Subsequently ion beam milling was carried out by using an ion milling system (model: Baltec RES 101) at 7 kV and low angle milling to attain specimen which are electron beam transparent. During ion milling Ar^+ ions were used for gentle thinning of the specimen without any damage for a few minutes. The density of the sample was measured using the conventional Archimedes principle was found to be 99% of its theoretical value. Thermal diffusivity measurements (Linseis, LFA 1000) were conducted on 12.7 mm diameter discs and rectangular bars 10X3X3 mm were used for electrical transport measurements (Ulvac, ZEM 3), in the temperature range from room temperature to 600 K. Specific heat measurements were performed using differential scanning calorimeter (Netzsch, DSC 404 F3). The accuracies in transport measurement are : ± 6% for thermal diffusivity, ± 10% for electrical conductivity, ± 7% for Seebeck coefficient, ± 8% for specific heat and ±0.5% for density.

3. Computational Details

The theoretical studies on Cu_3SbSe_3 are based on local density approximation (LDA) in DFT calculations, however, it has been reported earlier[32] that there is a significant improvement in the band structure observed employing generalized gradient approximation (GGA) as compared to using LDA. We have employed the all-electron-full potential linearized augmented plane wave (FP-LAPW) method to calculate the electronic band structure, density of states and transport properties of Cu_3SbSe_3. The FP-LAPW method is based on DFT and is implemented in the WIEN2K code.[33] We treat $3d^{10}4s^1$, $5s^25p^3$, and $2s^22p^4$ as valence electrons in Cu, Sb, and Se atoms, respectively. The Cu_3SbSe_3 crystal structure used to carry out DFT calculations is orthorhombic (P*nma*).[34] The

structure is mainly composed by two type of framework Cu-Se and Sb-Se with former providing the conduction path while the latter leads to distortion in the crystal symmetry. This complexity in crystal structure of Cu_3SbSe_3 would suggest a lower thermal conductivity.[35-37] The lattice constants and the atomic positions are taken from reference.[34] Keeping the lattice constants fixed at the experimental values, we have optimized the atomic positions so that the force on each atom is 1 mRy/au. The optimization is done with 36 k-points in the Irreducible Brillouin Zone (IBZ) and self consistent DFT calculations are performed on the optimized structure of Cu_3SbSe_3 with a self-consistent field tolerance of 10^{-4} Ry. The electronic exchange-correlation energy is treated by the GGA of Perdew-Burke-Ernzerhof (PBE).[38] The self-consistency is obtained using 100 k-points in the IBZ. The total and the angular momentum decomposition of the atoms projected electronic density of states (DOS) are calculated using a mesh of 432 k-points. The transport properties were calculated employing the BoltzTraP code[39] using 6900 k-points in IBZ.

4. Results and Discussions

The crystal structure of Cu_3SbSe_3 at room temperature was determined by conducting Rietvield refinement of the X-ray data using FullProf program. Fig. 1 show the XRD pattern of Cu_3SbSe_3 sample at room temperature, along with its Rietveld refinement, which suggests that the sample is single-phase crystallized in an orthorhombic structure with *Pnma* (62) space group with lattice constant a=7.98Å, b=10.61Å, c = 6.83Å, which is in complete agreement with that reported earlier by Pfitzner.[29] The sharp peaks in the XRD pattern indicate high cystallinity in the synthesized sample and the absence of any additional peaks suggests the phase purity of the synthesized Cu_3SbSe_3 sample. It may be noted that in the present study Cu_3SbSe_3 was synthesized at much lower temperatures using a solid-state reaction (320°C) in vacuum followed by reaction sintering

employing SPS (360°C), in contrast to the only existing report in the literature by Skoug et al.[17] who employed a melting route (850°C) followed by 72 hours of annealing.

A detailed microstructural characterization of Cu_3SbSe_3 sample employing HRTEM elucidated several interesting features in real and reciprocal space. A uniform microstructure is observed throughout the sample at low magnification (Fig. 2a). A grey-level contrast in the microstructure was evolved due to grain boundaries as well as thickness difference between the adjacent grains. However, these grains with densely-packed microstructure were discerned throughout the material. Inset A in Fig. 2a exhibits an atomic scale image of the encircled white-dotted region which reveals the stacking of two set of planes arranged perpendicular to each set. The inter-planar spacings of these 200 and 040 planes are 0.39 and 0.27 nm, respectively, which corresponds to Cu_3SbSe_3 orthorhombic crystal structure with the lattice constants: a = 0.79, b = 1.06 and c = 0.68 nm and space group *Pnma* (62). The reciprocal space interpretation of the microstructure was performed by recording the selected area electron diffraction pattern (SAED) shown in Fig. 2b, which clearly delineates this material to be of single-phase with good cystallinity. Moreover, a proper indexing exhibits that the diffraction pattern was oriented along [001] zone axis of orthorhombic crystal structure of Cu_3SbSe_3. A set of important planes, hkl: 040 and 200 are marked as diffraction spots 1 and 2, respectively, on the SAED (Fig. 2b).

An illustrative high resolution TEM micrograph, recorded at an atomic scale, displays a set of grains (marked as A to D in inset of Fig. 3) with interfacing boundaries. This figure suggests that individual grains are randomly oriented with inter-planer spacing's of 0.39, 0.33, 0.27, and 0.39 nm, corresponding to hkl values 200, 211, 040, and 200, for the grains marked from A to D, respectively (Fig. 3). However, at the grain boundaries the structure appears to be either amorphous or crystallographically disturbed to some extent. For instance, on the interface between grains A and B, a clear amorphous phase is marked by a set of arrows. The amorphous region between the grains B

to C is distinct with an average thickness of about 1.5 nm (marked with white dotted line). Boundaries between grains C and D and also between D and A are clearly marked by set of arrows, due to mis-orientation of atomic planes among these respective grains (Fig. 3). The formation of amorphous grain boundaries of ~ 1-2 nm thickness are known to occur in several pristine compounds.[40, 41] Fig. 3 further suggests that in some cases, the atomic scale imperfections are visible at some localized regions within an individual grain, which are clearly evident in grain A (encircled by white dotted lines). Similarly, in grain C, some lattice scale modulations are also apparent with a periodic spacing of about 1.2 nm.

FESEM image of Cu_3SbSe_3 shown in Fig. 4 reveals a uniform fine grained microstructure free from any visible residual porosity. The maximum densification post-sintering, achieved at a sintering temperature of 360°C under a pressure of 60 MPa employing SPS resulted in a densification of ~ 99%. This near-theoretical density is mainly due to the simultaneous application of pressure and a rapidly pulsated high dc current to the sample during SPS.[4, 42, 43]

The temperature dependence of electrical and thermal transport parameters of Cu_3SbSe_3 are shown in Fig. 5. Figure 5 (a) shows the experimental temperature dependence of α for Cu_3SbSe_3 along with the theoretically predicted curves, for different carrier concentrations. The positive value of the measured α indicates that the Cu_3SbSe_3 samples are p-type in nature. As is evident from Fig 5(a), α increases nearly-linearly with temperature and attains a value of 190 μVK^{-1} at 550 K. Figure 5(b), which shows the variation of σ with temperature, also exhibits a nearly-linear dependence on temperature and shows a value of 1400 S/m at 550 K, which is at least an order of magnitude lower compared to those observed in other state-of-the-art thermoelectric materials.[3] The low magnitude of σ may probably be due to its low carrier concentration, which was found to be 9.2 $X10^{19}$ cm^{-3}, measured using a lab-made Hall apparatus at 300 K. However, the σ can be enhanced by

incorporating suitable metallic dopants in Cu_3SbSe_3, which are known to migrate to network of grain boundaries of the matrix microstructure.[44] Despite a nearly-linear temperature dependence of σ and α, a change in slope is clearly evident at ~ 450 K (Fig. 5(a) & (b)), which is attributed to the order-disorder transition in this material as reported earlier.[25] This transition is also clear apparent in the temperature variation of specific heat, as shown in the inset of Fig. 5(c).

Figure 5(c) represents the temperature dependence of κ and κ_L of Cu_3SbSe_3. κ_L has been extracted by subtracting κ_e from and κ_e, which was determined by using Wiedemann-Franz law $\kappa_e = L_0\sigma T$, where the Lorenz number L_0=2.4 X 10^{-8} W Ω K^{-2}. The temperature dependence of κ, as shown in Fig. 6(c), was found to be different than reported earlier by Kirkham et al.,[25] for the same material, although a transition in C_p (inset) is clearly apparent at nearly the same temperature. Although the temperature variation of C_p is similar in the two studies, this discrepancy may be due to the difference in the temperature dependence of their thermal diffusivity owing to the vastly different temperatures employed in their synthesis. The measured value of κ for our Cu_3SbSe_3 samples was found to be 0.60 $Wm^{-1}K^{-1}$ at 300 K, which is lower than 0.7-1.0 $Wm^{-1}K^{-1}$ reported by earlier by Skoug et al.,[17] However, at 550 K this value of κ for our Cu_3SbSe_3 sample was found to be 0.26 $Wm^{-1}K^{-1}$, which is the lowest reported thus far this material at this temperature. This ultralow value of κ in Cu_3SbSe_3 has earlier been attributed to a combination of its complex crystal structure, very low Debye temperature and extreme anharmonicity of the lattice vibrational spectrum that gives rise to a large value Grüneisen parameter in this compound.[23] Owing to its ultralow κ, it was earlier suggested that Cu_3SbSe_3 compound could potentially be a good thermoelectric material.[17, 21] It is further evident from Fig 5 that κ is largely dominated by the phononic contribution with negligible contribution from the electronic part, as is generally the case for thermoelectric materials with intrinsically low thermal conductivity due to anharmonicity of the lattice phonons.[17, 23]

The ZT, calculated using the measured α, σ and κ data for our Cu_3SbSe_3 compound exhibits a very low value ZT (< 0.1) in the entire measured temperature range, which is contrary to the previously reported proposition.[17, 21] Nevertheless, this material could be a good potential thermoelectric material owing to its ultralow κ coupled with a moderate value of α, as the power factor can be tailored favorably by employing carrier concentration tuning employing suitable metallic doping.[30, 31] There have been several studies demonstrating how the transport phenomenon can be tuned by optimization of carrier concentration for further enhancement of ZT in existing high performance TE materials.[44-46] Kurosaki et al.,[45] observed an enhancement in ZT of AgTlTe by tuning the carrier concentration employing Cu doping. They observed a significant increase in power factor in AgTlTe without increasing the κ it with by doping 40 at% Cu, finally leading to a drastic increase in ZT from 0.3 to 0.6. Similarly the σ in Mg_2Si increases by several orders of magnitude on metallic doping resulting in an enormous increase in ZT by more than an order of magnitude.[31] The enhancement of the power factor of $AgGaTe_2$ through carrier concentration tuning has also been recently theoretically predicted[46] using density functional theory and Boltzmann transport theory. Several other strategies employed for the enhancement of power factor leading to enhancement of ZT in PbTe-based systems have been summarized by Rawat et al.[44, 47]

5. Computational Results

Our GGA calculations show that Cu_3SbSe_3 is a semiconductor with an indirect band gap of 0.47 eV. The total and the angular momentum decomposition of the atoms projected electronic density of states (DOS) are calculated using a mesh of 432 k-points was used. The transport properties were calculated with the BoltzTraP code[36] using 6900 k-points in IBZ.

The band structure is shown in Fig. 6(a). This compound shows an indirect energy gap of 0.47 eV located between Γ and U. Figure 6(b) shows the partial density of states of Cu1-d, Se2-p, Sb-s and

Sb-d. We find that the peak around -9 eV arises from the s-states of Sb. Inset of the figure shows density of states on a smaller scale for more clarity. The top of the valence band has major contributions from Cu1-d, Se2-p and Sb-s while the bottom of the conduction band arises from Sb-d states. We find a significant hybridization between Cu1-d, Se2-p and Sb-s from -3.0 eV to top of valance bands and Se2-p and Sb-s form -7.0 to -3.0 eV. The conduction bands are mainly Sb-d character. Earlier theoretical calculations by Sevic and Cagin[21], performed using LDA, resonate with our findings revealing indirect band gap of 0.24 eV. Dat Do et al.,[22] have also reported Cu_3SbSe_3 to be narrow indirect band gap semiconductor. The density of states curve shows large slope at band edges indicative of large α which reflects in our experimental findings (Fig 5(a)).

To substantiate the above measurements done for transport properties, we have also performed the transport properties calculations using GGA and then compared them with experimental values. Figure 5(a) shows the temperature dependence plots for α both measured and theoretically calculated for different doping concentrations of the order of 10^{19} cm^{-3}. The open circles are indicative of experimental values while different lines show values of σ, at different doping level. We have plotted four different concentrations of α and σ calculations against temperature to find out which one matches better. While performing calculations using BoltzTrap code, we have assumed a temperature independent relaxation time and have taken the value of τ to be 10^{-14} s.[48] The graph shows that α increases with temperature for all the samples in the entire temperature range for both theoretical and experimental case. The result shows that magnitude of α for experimental data points, which has highest value of 189 μV K^{-1} at 550 K, is in reasonable agreement with the calculated data plotted for different doping concentration in the entire temperature range.

Fig 5 (b), which displays both experimentally measured and theoretically predicted temperature dependence of σ, shows a pronounced decrease in σ with increasing temperature. The decrease in experimental σ could be attributed to the temperature dependence of τ, while for theoretical

calculations value of τ is taken as a constant, which could explain the visible difference between experimental and theoretical behavior of σ.

Conclusions

We present the first complete study on the synthesis, characterization and thermoelectric property evaluation of Cu_3SbSe_3. The material was synthesized employing a solid state reaction followed by spark plasma sintering and characterized for its phase structure and composition employing XRD, HRTEM, EDXS, SEM, XPS and DSC which confirm the formation of Cu_3SbSe_3 in a single-phase. The electrical transport measurements, suggest that Cu_3SbSe_3 exhibits a p-type behavior with moderate values of Seebeck coefficient (190 μVK^{-1} at 550 K). The electrical conductivity and Seebeck coefficient, evaluated theoretically using first-principle DFT calculations, show reasonable agreement with the experimentally determined values. The measured thermal conductivity is observed to be 0.26 $Wm^{-1}K^{-1}$ (at 550 K) and is the lowest reported for this material thus far and has main contribution from the lattice part. Despite a very low value of measured thermal conductivity the calculated ZT is found to be abysmally low (< 0.1), which is due its low electrical conductivity. Nevertheless, due to the environmentally friendly constituent elements coupled with its ultralow thermal conductivity Cu_3SbSe_3 could be a potential thermoelectric material as its power factor can be enhanced by tuning the carrier concentration by employing suitable metallic dopants.

Acknowledgements

This work was supported by CSIR-TAPSUN programme entitled *"Novel approaches for solar energy conversion under technologies and products for solar energy utilization through networking* - NWP54)*"*. The authors are grateful to the Director, Prof. R.C. Budhani, for his constant mentoring and support for this project. Thanks are also due to Prof. S.D. Mahanti for his valuable comments.

The technical support rendered by Mr. Radhey Shyam and Mr. Naval Kishor Upadhyay is also gratefully acknowledged.

Figure Captions:

Figure 1: XRD pattern of Cu_3SbSe_3 sample with Rietveld refinement. The red and black lines represent the observed and fitted data, respectively. The blue line represents the difference between the observed and fitted data.

Figure 2: HRTEM images of Cu_3SbSe_3, showing (a) bright field electron micrograph of a uniform densely packed microstructure. The inset A shows an atomic scale image of white-dotted encircled region (b) Selected area electron diffraction pattern of region C of Fig. 2(a)

Figure 3: HRTEM micrograph of Cu_3SbSe_3 showing different grains (A to D) with well defined crystallographic planes at an atomic scale. Inset: microstructure at low magnification elucidating different grains.

Figure 4: SEM micrograph showing surface topography of as-synthesized Cu_3SbSe_3.

Figure 5: Temperature dependence of transport properties of Cu_3SbSe_3. The open circles represent the experimental points and the colored lines depict the theoretically predicted curves, for different carrier concentration. (a) Seebeck coefficient. (b) Electrical conductivity (c) total thermal conductivity. The inset shows the temperature dependence of C_p.

Figure 6: (a) DFT results for band structure. Fermi level is indicated by E_F and (b) partial density of states as a function of energy. Inset shows a magnified view of this figure around the origin of X-axis.

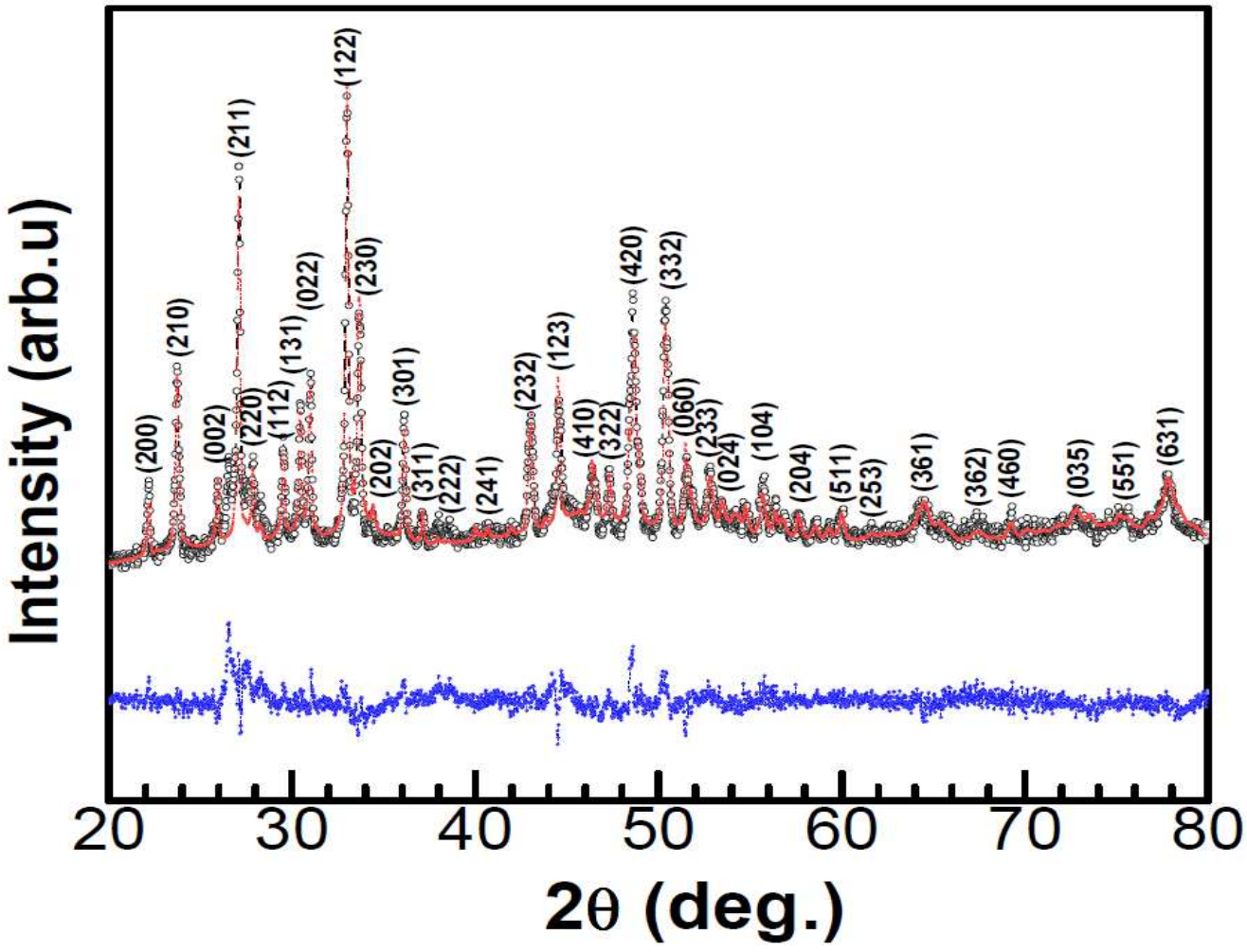

FIGURE 1

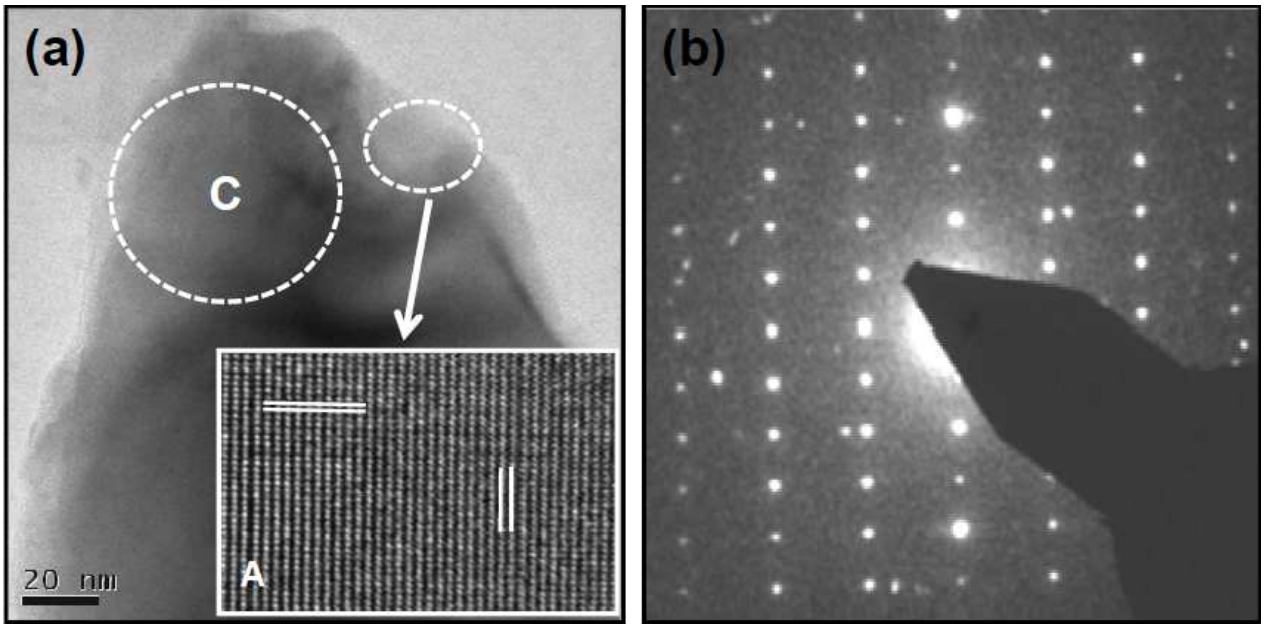

FIGURE 2

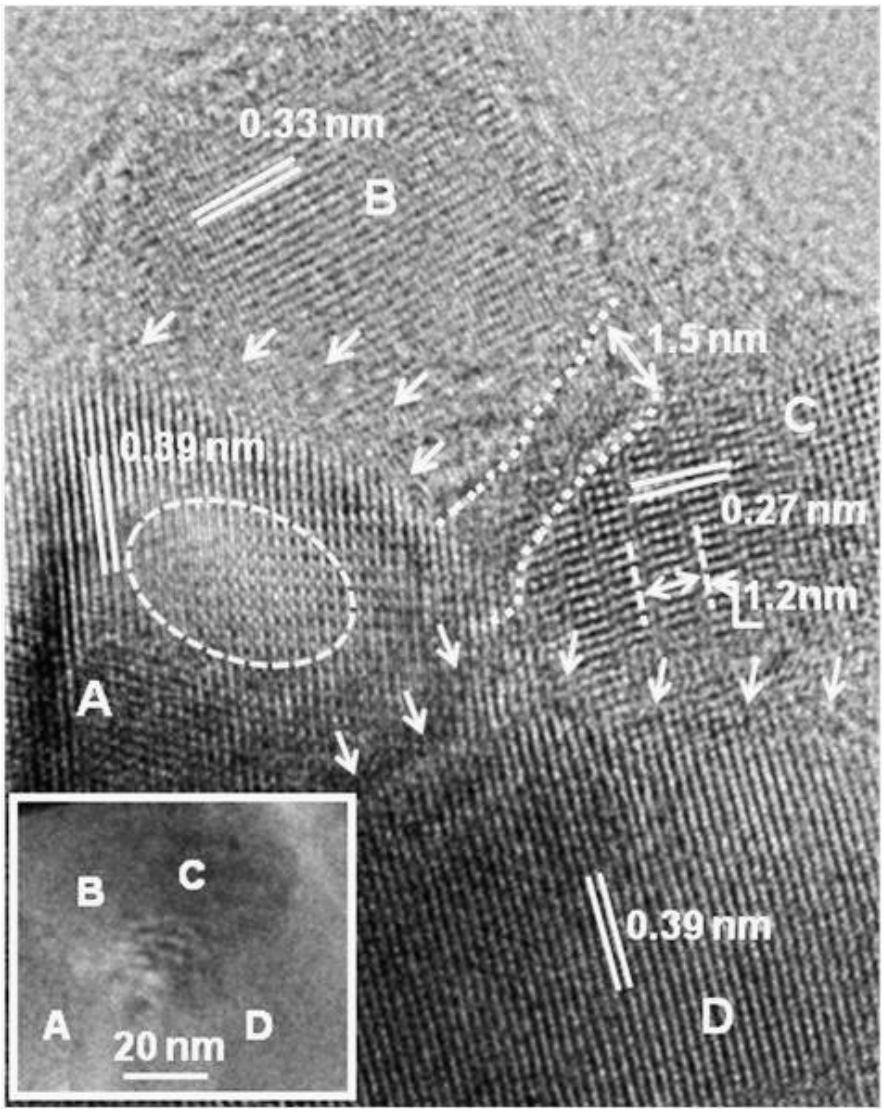

FIGURE 3

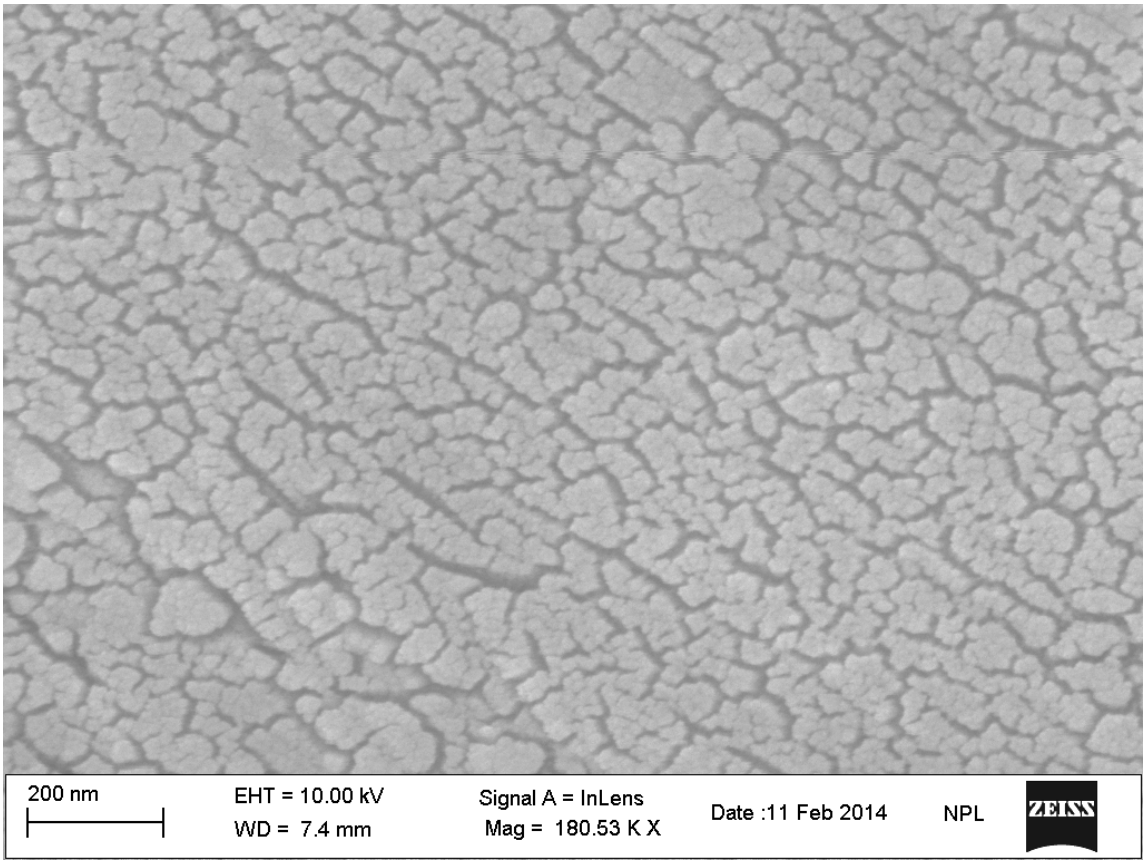

FIGURE 4

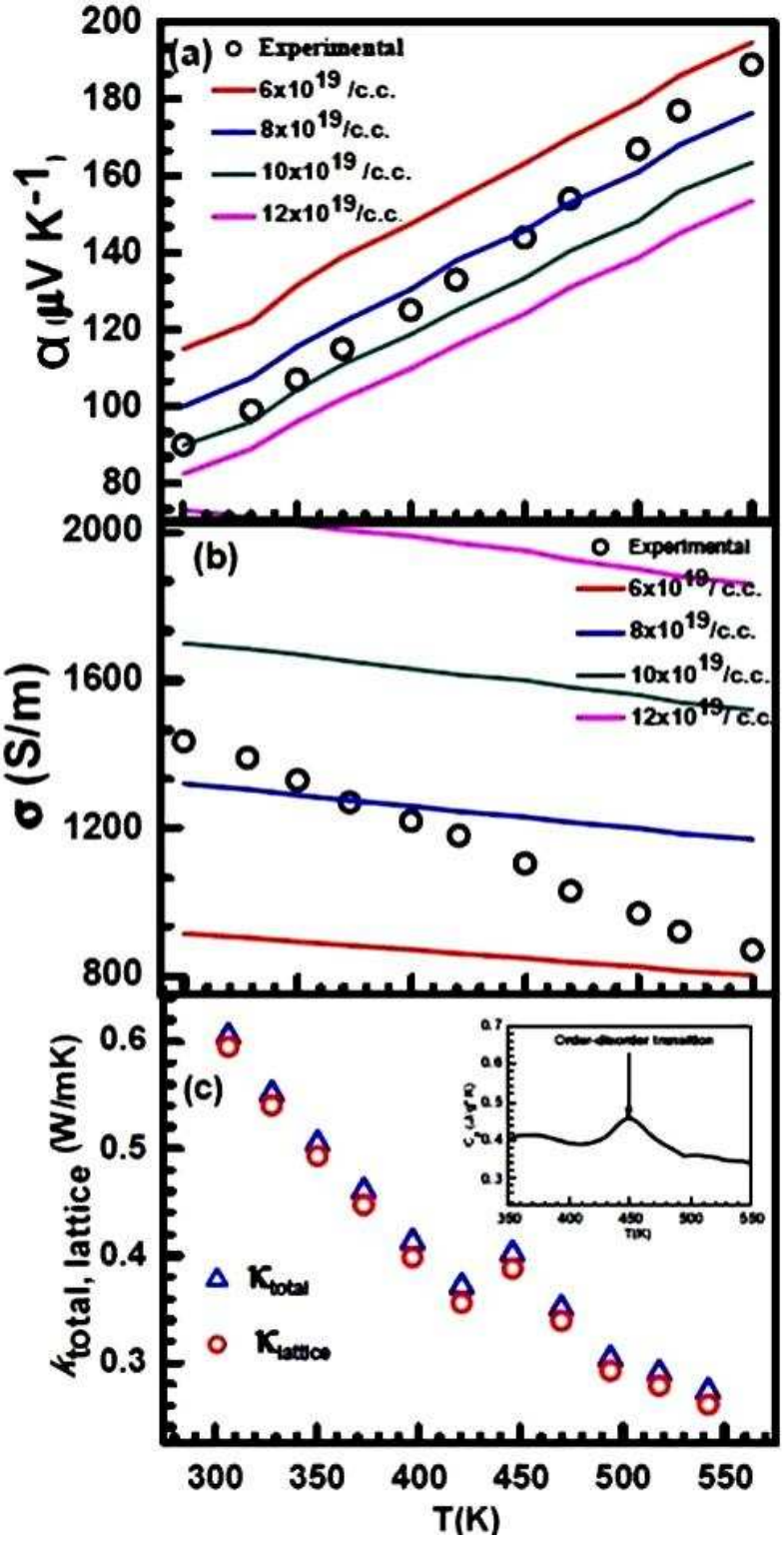

FIGURE 5

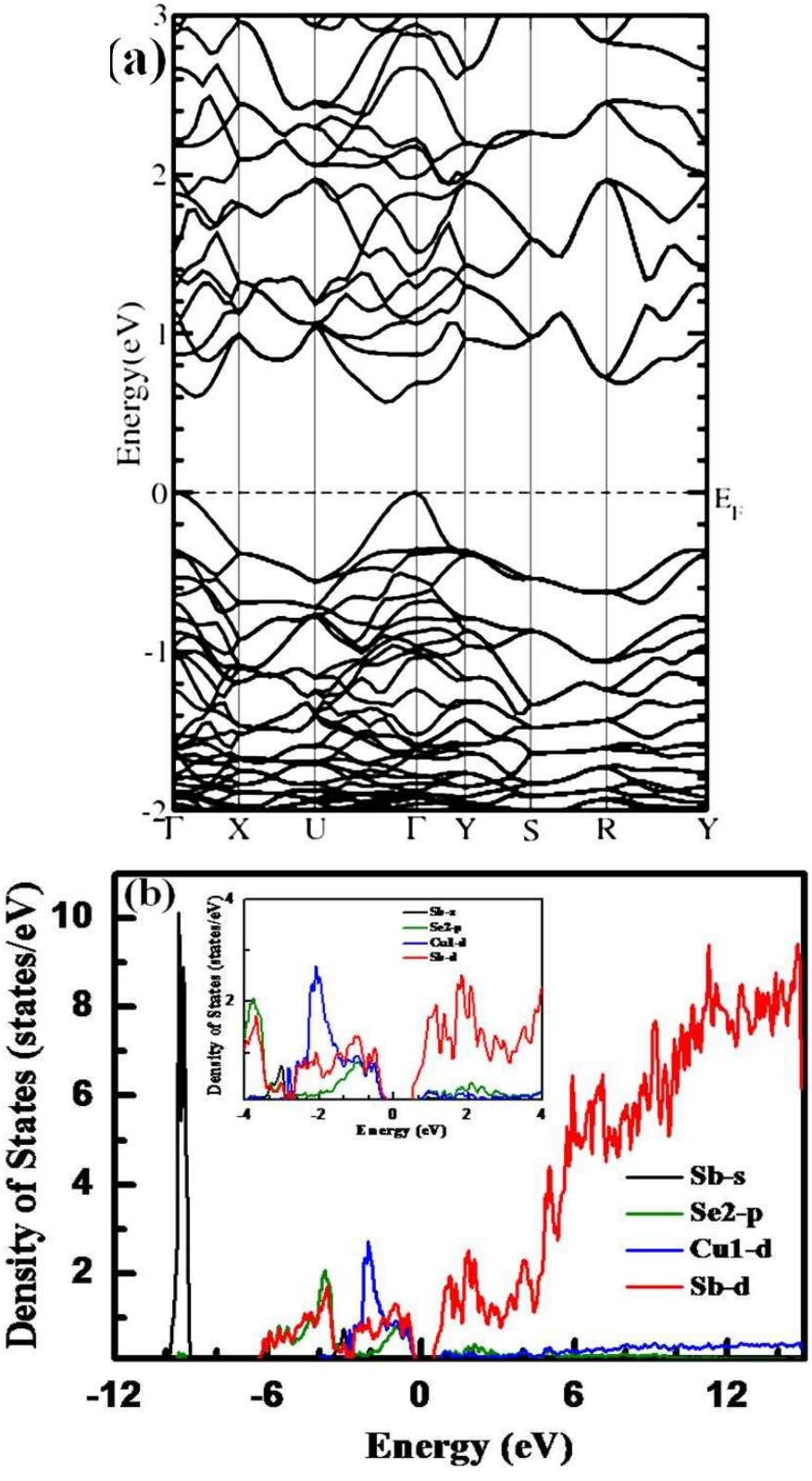

FIGURE 6 (a & b)

References

1. S. Ballikaya, H. Chi, J. R. Salvador and C. Uher, *Journal of Materials Chemistry A*, 2013, 1, 12478-12484.
2. J. R. Sootsman, D. Y. Chung and M. G. Kanatzidis, *Angewandte Chemie International Edition*, 2009, 48, 8616-8639.
3. G. J. Snyder and E. S. Toberer, *Nature materials*, 2008, 7, 105-114.
4. S. Bathula, M. Jayasimhadri, N. Singh, A. Srivastava, J. Pulikkotil, A. Dhar and R. Budhani, *Applied Physics Letters*, 2012, 101, 213902.
5. Y. K. Koh, C. Vineis, S. Calawa, M. Walsh and D. G. Cahill, *Applied Physics Letters*, 2009, 94, 153101.
6. L. P. Tan, T. Sun, S. Fan, R. V. Ramanujan and H. H. Hng, *Journal of Alloys and Compounds*, 2014, 587, 420-427.
7. W. Kim, J. Zide, A. Gossard, D. Klenov, S. Stemmer, A. Shakouri and A. Majumdar, *Physical Review Letters*, 2006, 96, 045901.
8. L. Hicks, T. Harman and M. Dresselhaus, *Applied Physics Letters*, 1993, 63, 3230-3232.
9. M. Dresselhaus, G. Dresselhaus, X. Sun, Z. Zhang, S. Cronin and T. Koga, *Physics of the Solid State*, 1999, 41, 679-682.
10. J. P. Heremans, C. M. Thrush and D. T. Morelli, *Physical Review B*, 2004, 70, 115334.
11. L. Hicks and M. Dresselhaus, *Physical Review B*, 1993, 47, 12727.
12. H. Wang, J.-F. Li, M. Zou and T. Sui, *Applied Physics Letters*, 2008, 93, 202103-202106.
13. K. Kurosaki, A. Kosuga, H. Muta, M. Uno and S. Yamanaka, *Applied Physics Letters*, 2005, 87, 061919-061919-061913.
14. F. Gascoin and A. Maignan, *Chemistry of Materials*, 2011, 23, 2510-2513.
15. Y. Aikebaier, K. Kurosaki, T. Sugahara, Y. Ohishi, H. Muta and S. Yamanaka, *Materials Science and Engineering: B*, 2012, 177, 999-1002.
16. D. Morelli, V. Jovovic and J. Heremans, *Physical Review Letters*, 2008, 101, 035901.
17. E. J. Skoug, J. D. Cain and D. T. Morelli, *Applied Physics Letters*, 2010, 96, 181903-181905.
18. L.-D. Zhao, S.-H. Lo, Y. Zhang, H. Sun, G. Tan, C. Uher, C. Wolverton, V. P. Dravid and M. G. Kanatzidis, *Nature*, 2014, 508, 373-377.
19. T. P. Hogan, A. Downey, J. Short, J. D'Angelo, C.-I. Wu, E. Quarez, J. Androulakis, P. F. Poudeu, J. R. Sootsman and D.-Y. Chung, *Journal of Electronic Materials*, 2007, 36, 704-710.
20. Y. Lan, A. J. Minnich, G. Chen and Z. Ren, *Advanced Functional Materials*, 2010, 20, 357-376.
21. C. Sevik and T. Çağın, *Journal of Applied Physics*, 2011, 109, 123712.
22. D. Do, V. Ozolins, S. D. Mahanti, M.-S. Lee, Y. Zhang and C. Wolverton, *Journal of Physics: Condensed Matter*, 2012, 24, 415502.

23. Y. Zhang, E. Skoug, J. Cain, V. Ozoliņš, D. Morelli and C. Wolverton, *Physical Review B*, 2012, 85, 054306.
24. D. T. Do and S. Mahanti, *Journal of Physics and Chemistry of Solids*, 2014, 75, 477-485.
25. M. Kirkham, P. Majsztrik, E. Skoug, D. Morelli, H. Wang, W. D. Porter, E. Andrew Payzant and E. Lara-Curzio, *Journal of Materials Research*, 2011, 26, 2001.
26. Y. Liu, J. Yang, E. Gu, T. Cao, Z. Su, L. Jiang, C. Yan, X. Hao, F. Liu and Y. Liu, *Journal of Materials Chemistry A*, 2014, 2, 6363-6367.
27. C. Yang, F. Huang, L. Wu and K. Xu, *Journal of Physics D: Applied Physics*, 2011, 44, 295404.
28. E. J. Skoug, J. D. Cain, P. Majsztrik, M. Kirkham, E. Lara-Curzio and D. T. Morelli, *Science of Advanced Materials*, 2011, 3, 602-606.
29. A. Pfitzner, *Zeitschrift für anorganische und allgemeine Chemie*, 1995, 621, 685-688.
30. Y. Pei, Z. M. Gibbs, B. Balke, W. G. Zeier and G. J. Snyder, *Advanced Energy Materials*, 2014.
31. S. Muthiah, J. Pulikkotil, A. Srivastava, A. Kumar, B. Pathak, A. Dhar and R. Budhani, *Applied Physics Letters*, 2013, 103, 053901-053905.
32. C. Stampfl and C. Van de Walle, *Physical Review B*, 1999, 59, 5521.
33. P. Blaha, K. Schwarz, G. Madsen, D. Kvasnicka and J. Luitz, *Local Orbitals Program for Calculating Crystal Properties*, 2001.
34. A. Pfitzner, *Zeitschrift für Anorganische und Allgemeine Chemie*, 1994, 620, 1992-1997.
35. G. A. Slack, *Solid state physics*, 1979, 34, 1-71.
36. A. Zevalkink, E. S. Toberer, W. G. Zeier, E. Flage-Larsen and G. J. Snyder, *Energy & Environmental Science*, 2011, 4, 510-518.
37. E. S. Toberer, A. F. May and G. J. Snyder, *Chemistry of Materials*, 2009, 22, 624-634.
38. J. P. Perdew, K. Burke and M. Ernzerhof, *Physical Review Letters*, 1996, 77, 3865.
39. K. Schwarz, P. Blaha and G. K. H. Madsen, *Computer Physics Communications*, 2002, 147, 71-76.
40. A. P. Tomsia and A. M. Glaeser, *Ceramic Microstructures: Control at the Atomic Level,* Springer, 1998.
41. L. Priester, *Grain Boundaries:From Theory to Engineering*, Springer, 2012.
42. S. Bathula, R. Anandani, A. Dhar and A. Srivastava, *Materials Science and Engineering: A*, 2012, 545, 97-102.
43. A. Bhardwaj, D. Misra, J. Pulikkotil, S. Auluck, A. Dhar and R. Budhani, *Applied Physics Letters*, 2012, 101, 169901-169903.
44. P. Rawat, B. Paul and P. Banerji, *Materials and Processes for Energy: Communicating current research and technological developments, Formatex Research Center,* 2013.
45. K. Kurosaki, K. Goto, H. Muta and S. Yamanaka, *Journal of Applied Physics*, 2007, 102, 023707.
46. H. Peng, C. Wang and J. Li, *Physica B: Condensed Matter*, 2014, 441, 68-71.
47. P. K. Rawat, B. Paul and P. Banerji, *physica status solidi (RRL)-Rapid Research Letters*, 2012, 6, 481-483.
48. N. Ashcroft and N. Mermin, *Solid State Physics, Saunders College, Philadelphia, Pennsylvania*, 1976.

Graphical Abstract

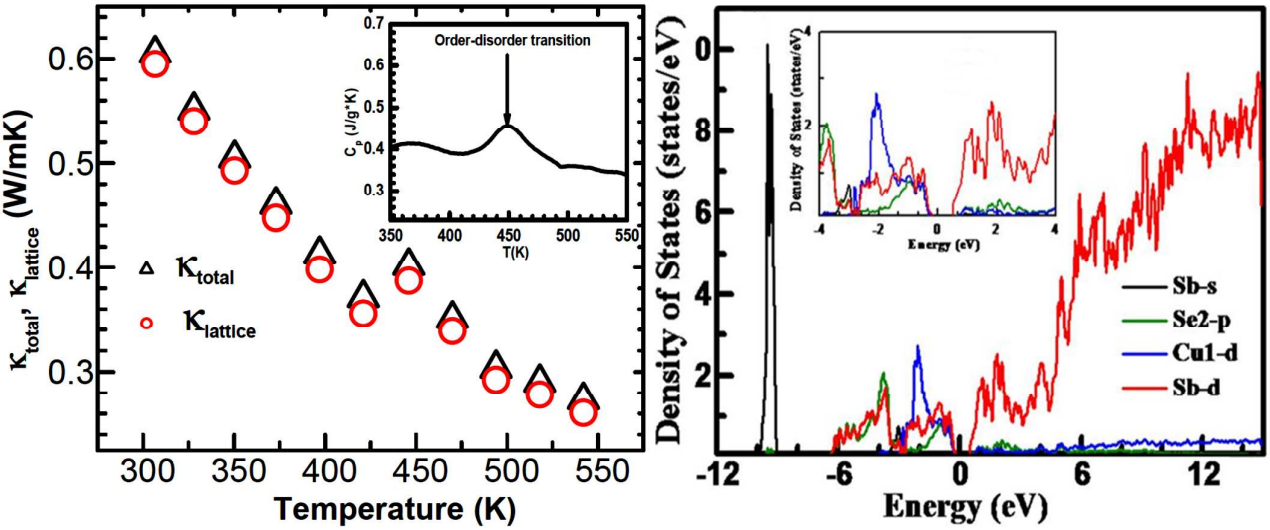

Novelty of the work

Intrinsically ultra-low thermal conductivity and electrical transport in single-phase Cu_2SbSe_3 synthesized employing solid state reaction and spark plasma sintering.